Design and Optimization of Permanent Magnet Based Adhesion Module for Robots Climbing on Reinforced Concrete Surfaces

M.D. Omar Faruq Howlader and Tariq Pervez Sattar

Abstract In this chapter, the detailed design of a novel adhesion mechanism is described for robots climbing on concrete structures. The aim is to deliver a low-power and sustainable adhesion technique for wall climbing robots to gain access to test sites on large concrete structures which may be located in hazardous industrial environments. A small, mobile prototype robot with on-board force sensor was built which exhibited 360° of manoeuvrability on a 50 × 50 mm meshed reinforcement bars test rig with maximum adhesion force of 108 N at 35 mm air gap. The proposed adhesion module consists of three N42 grade neodymium magnets arranged in a unique arrangement on a flux concentrator. Finite Element Analysis (FEA) is used to study the effect of design parameters such as the distance between the magnets, thickness and material of the flux concentrator, use of two concentrators, etc. Using two modules with minimum distance between them showed an increase of 82 N in adhesion force compared to a single module system with higher force-to-weight ratio of 4.36. An adhesion force of 127.53 N was measured on a real vertical concrete column with 30 mm concrete cover. The simulation and experimental results prove that the proposed magnetic adhesion mechanism can generate sufficient adhesion force for the climbing robot to operate on vertical reinforced concrete structures.

1 Introduction

Non Destructive Testing (NDT) plays a vital role in ensuring the safety and integrity of capital assets. NDT techniques have found application in the regular inspection of large safety critical infrastructures to determine their structural integrity and to plan maintenance and outage schedules. The applications range from large welded steel structures [1] (such as petrochemical steel storage tanks, ship hulls, pressure vessels, etc.) to composite structures (such as wind blades and modern aircraft wings and fuselage) and to concrete structures (such as cooling towers of power plant, bridge columns, dams, nuclear power plants buildings, etc.). While concrete can offer

M.D.O. Faruq Howlader (✉) · T.P. Sattar
Robotic and NDT Research Centre, London South Bank University, London, UK
e-mail: howladem@lsbu.ac.uk

Y. Bi et al. (eds.), *Intelligent Systems and Applications*,
Studies in Computational Intelligence 650, DOI 10.1007/978-3-319-33386-1_8

higher strength and durability compared to other building materials [2], atmospheric moisture and chlorides cause the concrete structures to lose their strength. Therefore, from a civil engineering perspective, NDT plays a critical role in detecting induced structural faults like reinforcement bar corrosion, cracking, and delamination of the concrete surface [3].

Currently, the NDT of concrete structures is mostly performed manually. The primary challenge of carrying out the procedure on a vertical concrete structure is to gain access to the inspection area which is normally located at a high altitude. The NDT of these vertical concrete structures must be addressed by ensuring the safety of operators, increasing the inspection speeds and hence decreasing the time taken to inspect them, and improving the quality of NDT measurements which suffer as a result of operator fatigue when performing NDT on large surfaces. The inspection speeds and cost reductions can be dramatically improved by using climbing robots to gain access to a test site by eliminating the need to erect scaffolding or make lengthy preparations to abseil down or use suspended platforms. The quality of NDT data can be improved by using automated robotic deployment of NDT sensors thereby eliminating human factors such as fatigue or inattention. As a result, climbing robots in the field of vertical structures are of increasing importance for inspections and maintenance tasks. A considerable amount of research has been devoted to develop various types of experimental prototypes for industrial inspection tasks with the application mostly dictating the design aspects of climbing robots [4, 5].

This chapter focuses on the development of a novel wall-climbing robot to carry out the Non-Destructive Testing (NDT) of safety critical reinforced concrete structures using permanent magnets to adhere to the structure. Permanent magnet systems do not require the supply of energy and hence have an inherent advantage for climbing robots.

The arrangement of multiple permanent magnets on the back of a flux concentrator provides a unique mechanism to concentrate and magnify the magnetic energy to couple with reinforcement bars (rebars) buried under the concrete surface. The research aim is to optimize the design parameters to provide increased payload capacity.

The chapter consists of eight sections. Section 2 gives an overview of the working environment of the mobile robot. Section 3 presents a review of the state-of-the-art of climbing robots. Section 4 specifies the design requirements of the climbing robot for successful deployment while Sect. 5 details the simulations carried out using Finite Element Analysis (FEA). Development of the prototype climbing robot is presented in Sect. 6 and the experimental results to validate the design are discussed in Sect. 7. The chapter concludes with a brief summary and recommendations in Sect. 8.

2 Current Practices to Access Vertical Structures

The current practice is to carry out manual NDT of large, vertical, safety critical structures and the biggest task in the performance of manual NDT is to first obtain access to test sites. This is mostly obtained by constructing scaffolding. The scaf-

Fig. 1 Manual NDT of weld lines on cargo container ships

foldings used are of two main types, fixed type and abseiling type. A fixed type scaffolding can offer stable access of the target area to the NDT operator. However, this type of scaffolding is expensive and time-consuming to erect and disassemble. The abseiling type is most commonly used for inspection purposes and is less expensive and time consuming than its fixed counterpart. But it is more vulnerable to wind gusts, bad weather and accidents [6]. A case study to show the problems of erecting a fixed scaffolding to inspect a 300 foot tall chimney is described in [7]. Figure 1 shows a scenario of manual NDT of approximately 0.5 Km of vertical and horizontal weld lines during the construction of new-build cargo container ships by erecting scaffolding consisting of wood planks and ropes.

However, for more complex structures such as bridge columns, decks, and concrete storage tanks etc. scaffolding is not a feasible option. In those cases, access devices like cranes and gondolas are deployed to the desired position. Sometimes professional climbers, called 'spider workers', are involved in the inspection if the structure cannot be accessed otherwise.

Other than the complexity, safety of the NDT operators and the cost of preparations are the two main issues that must be considered. Here the operators deal with hazardous working environments with possibly limited manoeuvrability [8]. More often than not, it's the working environment that causes the most concern rather than the altitude. In the nuclear industry for example, the spider-workers are exposed to radioactive air while inspecting concrete reactor tanks. Even though the nuclear regulatory commission has determined 50 mSv of radiation exposure in a year as a safe limit [9], it is the cyclic exposure to radiation that proves fatal. In 2015, a report in the British Medical Journal stated that, a total of 17, 957 workers in the nuclear industry from France, the United Kingdom, and the United States died from solid cancers caused by low level but cyclic radioactive exposure in the last 72 years [10].

Likewise, in the chemical industry, the operators have to deal with high temperatures as a boiler tube is shut down for inspection, it requires 2–3 days before it reaches a safe level [11]. In addition, in many of these inspection tasks, the freedom of movement is very restricted and the operator mobility is very low with the result

that the NDT inspection is of poor quality. Therefore, interest in the development of climbing robots has grown significantly as robotic solutions can offer quick access to tall structures and remote test sites leading to increased operational efficiency, reduced cost and greater health and safety protection to human operators.

3 Climbing Robots—A Design Review

The workplace of climbing robots is on the vertical plane, therefore, it requires adhesion mechanisms to carry its payload along different types of vertical surface. The robot is required to support its own body weight as well as carry a given payload while climbing. A review of climbing methods based on locomotion and adhesion mechanisms is presented.

3.1 Adhesion Types

Permanent magnets have been used as the adhesive method when designing robots that are required to climb ferrous surfaces for a long period. The "WCR System" [12] is an example of a wall climbing robot developed by a team from Cambridge University. The application of the robot was to label the scale of steel oil storage tanks. Later a number of robots were developed and patented based on the same principle. A non-contact magnetic adhesion mechanism proposed in [13] implemented arrays of magnets under the chassis of the robot as shown in Fig. 2a. A constant gap of 5 mm between the magnet and the wall surface was maintained. The effect of multiple magnet layers and the distance between the magnets on the total adhesion force are not investigated in that study. Another permanent magnet based tracked robot presented in [14] investigated the effect of air gap between multiple magnets and the steel surface. The robot consisted of an aluminium frame and track wheels with permanent magnets located on the steel channels. The track wheels and the magnet attachment are shown in Fig. 2b. The effect of distance between the magnets, and the effect of magnet dimension on the overall adhesion force have not been investigated.

Another robot [15] was developed based on the magnetic wheel system. In this case, the wheel was constructed of magnetic material and the effect of different wheel rims on the distribution of magnetic flux lines was investigated on both planer and curved surfaces. The robot can achieve 60 N of maximum adhesion force while climbing a ferrous surface.

The most frequent approach to adhesion on a surface is to implement suction and pneumatic adhesion. These systems are mainly used for non-ferromagnetic, non-porous, relatively smooth surfaces, and can be applied to a large suction area to increase the adhesion force. Examples of robots using suction are a climbing robot for inspecting nuclear power plants [16], a robot using tracked wheel mechanism with suction pads [17] and two other four limbed robots with suction pads attached

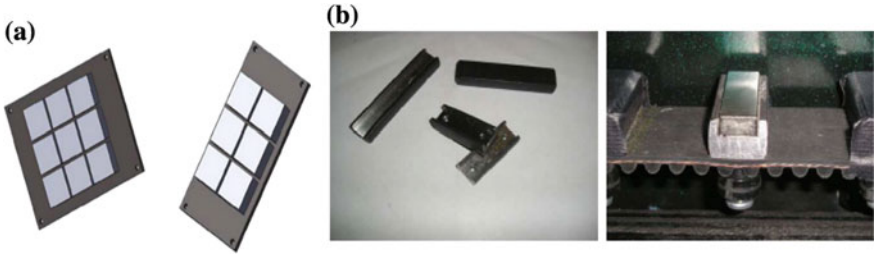

Fig. 2 **a** Arrays of rare earth permanent magnets on steel plates as proposed in [13]; **b** Tracked wheels and magnet spacing as in [14]

[18]. The initial limitation of the suction mechanism is that it requires time to develop enough vacuum to generate sufficient adhesion force and as a result, the speed of the robots using suction is relatively low [19]. To solve this problem a vacuum rotor package called Vortex generates a low pressure zone enclosed by a chamber [20]. The high speed rotor causes the air to be accelerated toward the outer perimeter of the rotor and away from the centre radially. The resulting air exhaust is directed towards the rear of the robot and creates an adhesion towards the climbing surface. However, the resultant adhesion force from vortex technology is not enough to support a reasonable payload. Moreover, as the gap between the climbing surface and the chamber is required to be absolutely minimized, robots using vortex technology cannot offer floor-to-wall transitions.

Researchers have also investigated the application of biological agents in robot design. The Lemur II is an example of such design [21]. It can climb vertical rough surfaces with the help of four limbs. Another example of this design is the RiSE robot which imitates the movement of a Hexapod [22] using a special type of micro spine attached to its six legs. A more advanced robot based on the same design principle is CLIBO [23] that uses 16 motors for high manoeuvrability. A robot design derived from human climbing behaviour was developed named the ROCR [24]. It consists of two modules and a tail that thrusts sideways and propels the robot upwards on a rough vertical surface.

3.2 Locomotion Types

For locomotion, wheel-type, track-type, wire and ligament based locomotion mechanisms are used to build robots for inspecting complex shaped structures with high mobility. The benefit of a wheel-type mechanism is that it can move and turn flexibly with a small contact surface between the wheels and the wall. Therefore, the robot's energy-use ratio is low. However, wheeled robots with suction type adhesion need to maintain a fixed minimum air gap to sustain the adhesion and this creates problems with loss of adhesion when climbing uneven surfaces. Also, these wheels cannot overcome larger steps, so they are exposed to slip effects.

The track-type mechanism has a larger contact area and can generate higher attraction force and it can move well in one direction but finds it is hard to change direction since it has only two degrees of freedom.

Wires and rail locomotion can be used to move a robot up vertical tall structures for some fixed applications like maintenance and cleaning. A tile-wall robotic system [25] for the NDT of concrete buildings is a good example of this sort of climber. This system consists of a portable module carrying NDT devices, with a ground and a roof platform connected together by a conveyor belt. The advantage of this mechanism is that the control system only has to position the NDT sensors at the point required and the additional payload is carried and held by the conveyor belt. Even though this system allows much simpler robot dynamics, the system is ineffective in the case of very tall structures as very long conveyor belts need to be installed between the roof and the ground.

The suction cup option is the most widely used method for non-magnetic surface climbing robots in comparison to other adhesion mechanism reported in the literature. Traditionally, vacuum pumps, often in the form of suction cups, are used as vacuum producers. They can produce high vacuum and large suction force. However, when suction cups and vacuum pumps are applied to a wall-climbing robot, other pneumatic components such as solenoid valves and regulating valves are also needed [23] which increase the weight of the robot especially when high flexibility of locomotion is required. Adhesion principles of vortex and electro adhesion are still in the development stage and not completely understood. As a result, few practical products have been developed for reinforced concrete surfaces, though wall-climbing robots have been researched for many years.

4 Design Requirements

The permanent magnet adhesion climbing robot discussed in this chapter is designed to deliver a solution to deploy a variety of NDT equipment on a robotic platform. A specific set of requirements can be postulated suitable for this task.

- Climbing capability—The robot must have a climbing capability on vertical reinforced concrete surfaces of up to 50 m high and curved surfaces with a minimum diameter of 10 m. This kind of structure is common for concrete buildings in nuclear power plants.
- Magnetic adhesion penetration depth—Concrete is a brittle material that can absorb strong compression forces but breaks at very low tensile forces [26]. Cracking and delamination can occur on non-reinforced concrete structures if excessive force is induced by external loading as shown in Fig. 3. To counter the excessive tensile force, concrete structures are reinforced with strong materials like steel reinforcement bars (rebars). Nuclear and other safety critical structures are reinforced with the dense meshing of rebars using special techniques to distribute the concrete as it is poured [27].

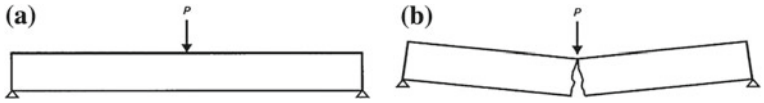

Fig. 3 Crack occurrence on a concrete slab **a** Bending Force < Tensile threshold force, **b** Bending Force > Tensile threshold [26]

As steel rebars are highly ferromagnetic, therefore magnetic coupling with the buried rebars can deliver a simple, low-energy adhesion mechanism. The main challenge is to shape and concentrate magnetic flux to penetrate the concrete cover as deeply as possible to gain sufficient magnetic adhesion. The nominal concrete cover for different environmental exposures is regulated by the BS 850 and Eurocode and is determined by concrete quality and intended working life of the structures [28]. To meet these standards, the proposed magnetic adhesion module is required to ascend on vertical nuclear buildings with an NDT payload by generating sufficient adhesion force while magnetically coupling with rebars at 45 mm depth. The following requirements must be satisfied:

- Dynamic force—A dynamic force analysis can determine the stability of the robot while climbing on vertical or inclined surfaces. This will also define the minimum adhesion force required to avoid sliding and roll-over failure. If the robot's weight is G, the wheels friction coefficient is μ, h is the height of the centre of gravity from the climbing surface, L is the distance between the front and back wheel, robot mass acceleration is m and a respectively then according to [29], adhesion force, F_a required to avoid sliding is

$$Fa \geq (G + ma)/\mu \tag{1}$$

  And for roll-over avoidance,

$$Fa \geq \frac{G \times h}{L} \tag{2}$$

- Payload capacity—A variety of NDT sensors such as Ground Penetrating Radar (GPR), thermo graphic sensors, cover meter, Wenner probe etc. are used for concrete inspection. Depending on the application of the robot and the type of sensors used, a payload capacity of maximum 5 kg is required for safe operation during robotic inspection. Moreover, the robot weight should be kept to a minimum. In case of any adhesion failure, the impact of a heavy robot would cause damage to the plant equipment and surroundings which must be avoided.
- Reliability and safety—The safety and reliability of the robot must be ensured by robust hardware and mechanical design. A practical solution would secure the mobile robot with a safety harness with provision of power and NDT and control data transmission with an umbilical cable.

Ultimately, a strong and secure adhesion mechanism is the pinnacle of design requirements. The adhesion mechanism defines the system reliability and payload capacity.

5 Parametric Studies of the Adhesion Module

The proposed adhesion module is comprised of several magnets and a flux concentrator called the 'yoke'. The adhesion module, air gap and the steel rebar constitute a magnetic circuit as shown in Fig. 4. In order to achieve a target adhesion force, parametric studies of the adhesion module's design criteria such as material and thickness of the yoke, effect of rebar mesh on adhesion and use of multiple yokes have been carried out using Finite Element Analysis (FEA) software Comsol Multiphysics. The main properties of the materials used in the simulations are listed in Table 1.

The primary aim is to achieve maximum adhesion force to support the payload by using a minimum number of magnets. The ratio of the adhesion force and net weight of the system, η determines the module's performance by achieving maximum adhesion force F_a from the minimum net weight of the system W. Therefore,

$$\eta = Fa/W \tag{3}$$

5.1 The Influence of Distance Between Magnets

The initial dimensions used are magnet length, $M_l = 50$ mm, width, $M_w = 50$ mm, thickness, $M_t = 12$ mm, rebar diameter, $R_d = 12$ mm, yoke thickness, $Y_t = 10$ mm; concrete cover, $C_c = 35$ mm and the distance between the magnets is chosen as variable. With the distance varied from 10 mm to 150 mm, the adhesion force increases

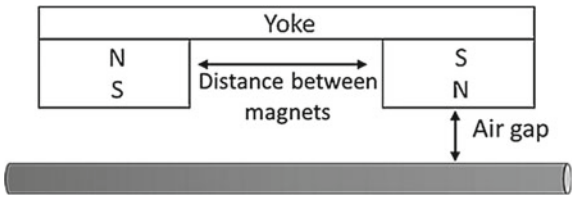

Fig. 4 Block diagram of the magnetic circuit

Table 1 Material properties used for Comsol simulations

Properties	Value
Magnetic induction intensity B_r (T)	1.31
Coercive force H_{cb} (KA/m)	915
Intrinsic coercive force H_{ci} (KA/m)	955
Magnetic energy product HB (KJ/m^3)	318
Relative permeability (μ_r)	1.05
Relative permeability of yoke (μ_r)	5000
Relative permeability of concrete surface (μr)	1
Relative permeability of steel rebar (μr)	1500

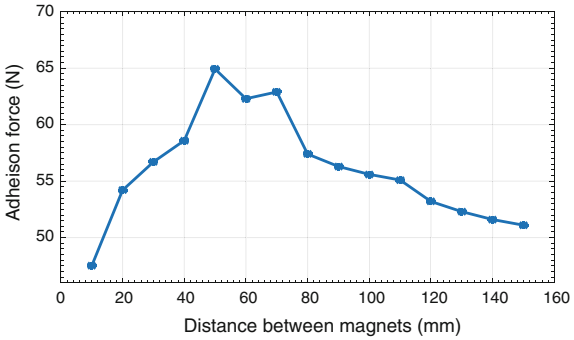

Fig. 5 Simulated adhesion force at different distances between magnets

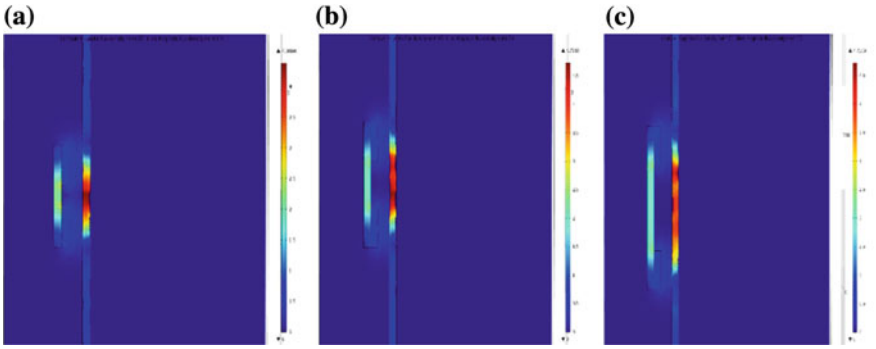

Fig. 6 Magnetic flux concentration norm at different distance between magnets; **a** Distance: 10 mm, **b** Distance: 50 mm, **c** Distance: 150 mm

rapidly at the beginning from 47.5 N to 64.93 N with the maximum at 50 mm distance as shown in Fig. 5. With the two magnets close to each other, the resultant magnetic attraction area is small. The biggest attraction area is indicated by the red hotspots at 50 mm in Fig. 6b which indicates the optimum distance between the magnets for a maximum adhesion force. At distances greater than 50 mm, the magnetic flux density along the rebar length starts to decrease and there is a gradual fall in the resultant adhesion force to 51.38 N at 150 mm distance between magnets.

5.2 Magnetic Circuit Coupling Optimization

Building the adhesion module with multiple magnets influences the magnetic flux distribution and the adhesion force. Previously, one magnetic circuit travelling from North Pole of one magnet to the South Pole of the other magnet was built using two magnets. To increase the number of magnetic circuits using additional magnets, two other arrangements as shown in Fig. 7 are investigated here.

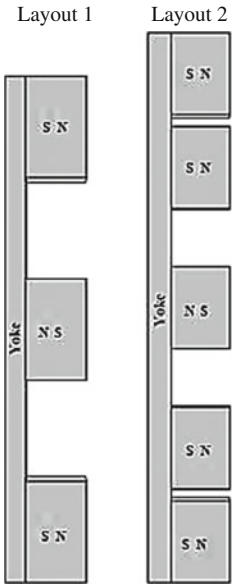

Fig. 7 Proposed magnetic circuit coupling layouts

It can be observed from Fig. 8a that, both layout 1 and layout 2 generates higher adhesion force than the method used in the previous section. At 10 mm concrete cover, resultant adhesion force is 312.57 N and 451.33 N respectively for layout 1 and 2. But as the concrete cover is increased to 20 mm, adhesion force reduces to 188.02 N and 248.17 N respectively i.e. a reduction of 39.84 % for layout 1 and 45 % for layout 2. Therefore, the rate at which adhesion force falls as the rebar distance increases is lower for layout 1 than layout 2. However, extra additional force generated by the layout 2 yields in higher values of η compared to the layout 1 which negates the additional weight of the extra magnets. The comparative values of η are shown in Fig. 8b.

Moreover, magnetic flux density norm shows that as two North Poles are located in close proximity at both ends of the adhesion module in case of layout 2, it does not concentrate magnetic flux as uniformly as layout 1. Therefore, layout 2 would be more applicable in cases where magnetic coupling with more than one layer of buried rebars is desired and layout 1 would be more suitable if the rebars are located at a lower depth. For the remainder of this chapter, layout 1 has been considered because of uniform distribution of magnetic flux.

5.3 Effect of Yoke Thickness and Material

The adhesion force generated by layout 1 without any yoke is 58.34 N while adding a 10 mm thick iron yoke increases the force to 83.71 N for 35 mm of concrete cover.

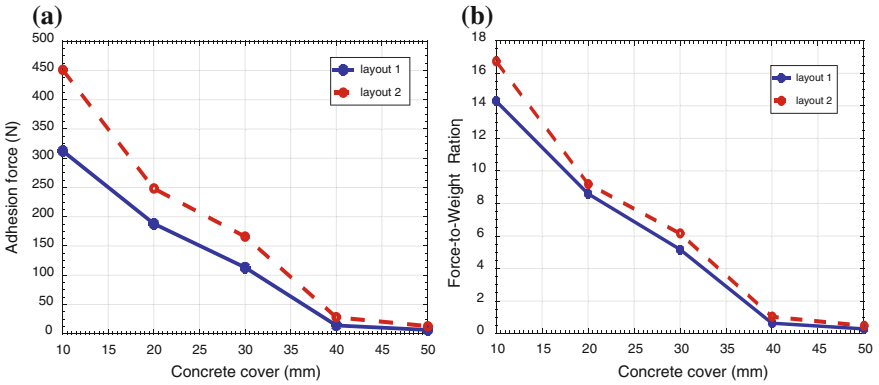

Fig. 8 **a** Comparison of adhesion force and **b** force-to-weight ratio between layout 1 and layout 2 for different concrete cover

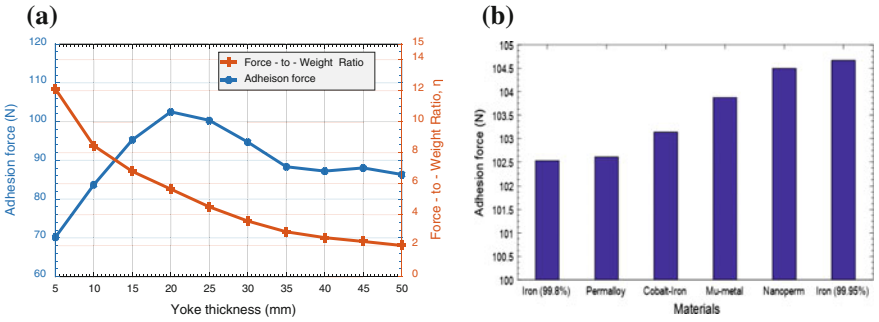

Fig. 9 Adhesion force comparison for: **a** different yoke thickness; **b** different materials

Therefore, the thickness of yoke plays a critical part to maximize adhesion force. To investigate this parameter further, models with varied yoke thickness from 5 mm to 50 mm are simulated. All other parameters are kept the same as in previous simulations. According to the results in Fig. 9a, adhesion force would increase significantly to 102.53 N for yoke thickness of 20 mm. Moreover, the magnetic flux leakage is lower in the yoke's opposite surface and more flux lines are concentrated toward the rebar shown. However, the adhesion force comes to a saturation point of approximately 85 N at 35 mm yoke thickness, where further increases in yoke thickness would not have any significant influence on the adhesion force but η value begins to decrease. The main reason for this is that when the yoke thickness reaches a certain value, the magnetic flux concentration is too small towards the rebar to influence the adhesion. Furthermore, adhesion force measurements for 20 mm thick yokes of different materials shows that the value of magnetic permeability has negligible influence on adhesion force as results are shown in Fig. 9b.

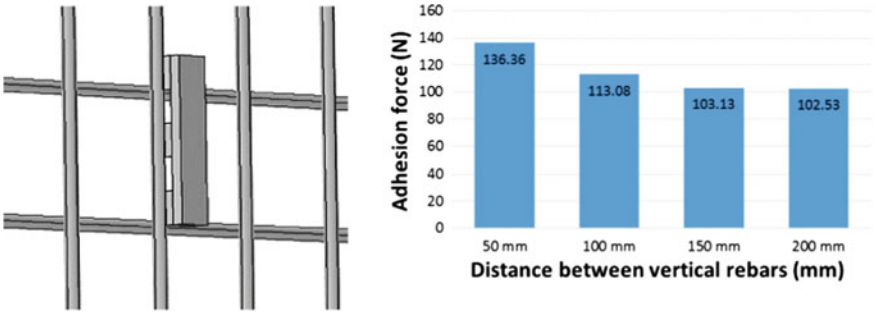

Fig. 10 Simulation setup of rebar mesh and resultant adhesion force at different mesh settings

5.4 *Effect of Rebar Mesh*

In practice, different spacing between the rebars is used depending on the concrete structure. The adhesion force for a rebar mesh with different spacing is presented here. In the simulation model, the distance between horizontal rebars is set to 150 mm which is the industry standard [28] and the distance between the vertical rebars is varied from 50 mm to 200 mm while keeping the concrete cover constant at 35 mm.

The simulated adhesion force measurements in Fig. 10 show that the adhesion force is increased as the distance between the vertical rebars is reduced. This is because in case of two rebars close together, magnetic flux can act on a larger area and generate bigger force compared to a single rebar. In case of safety critical infrastructures, the rebars are meshed at a distance of 50 mm for greater strength and longevity and this novel adhesion mechanism is much more suited to those environments.

5.5 *Effect of Multiple Yokes*

As structures are reinforced with a mesh of rebars therefore implementation of multiple yokes can increase the attraction area and ultimately generate higher adhesion force. To investigate this further, models are built using two layouts as in Fig. 11 and the adhesion force is measured for different distances between them. Rebar meshing of 50 mm × 50 mm is considered for this setup.

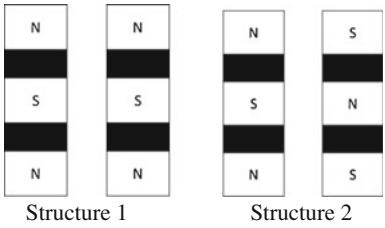

Fig. 11 Two proposed coupling structures using multiple yokes

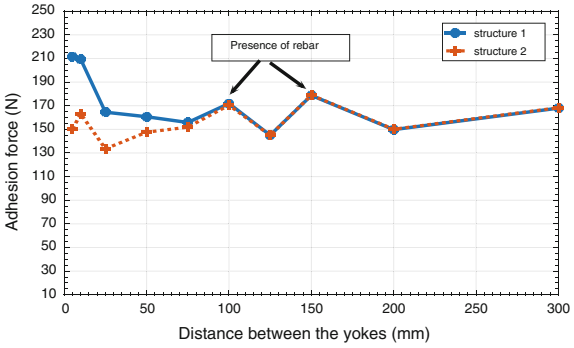

Fig. 12 Adhesion forces at different distances between the yokes for both structures

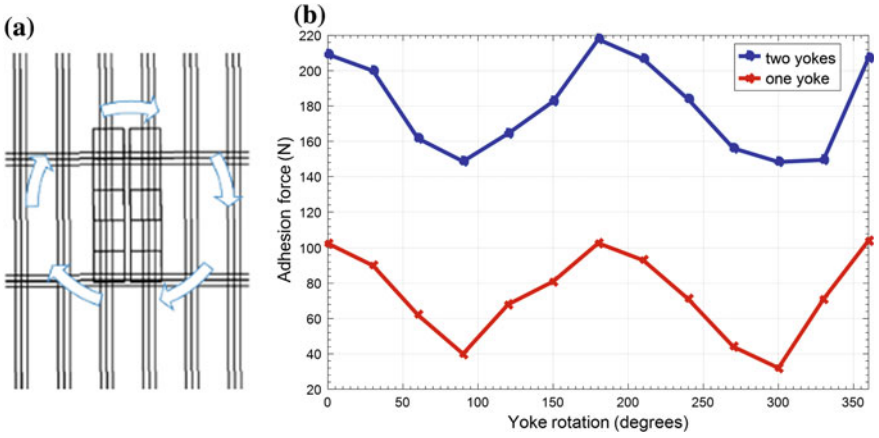

Fig. 13 Comparison of adhesion forces at different rotational positions of adhesion modules consisting of one and two yokes: **a** Simulation setup; **b** Resultant adhesion forces

Results in Fig. 12 show that, structure 1 provides higher adhesion force compared to structure 2 when the distance between yokes is minimized. At 5 mm distance, structure 1 generates 211.7 N of force compared to 150.3 N for structure 2. The adhesion force decreases as the distance is increased to 50 mm. At distances higher than 50 mm, both structures generate exactly the same amount of adhesion force as seen in Fig. 12. Moreover, an increase of adhesion force to 188 N is seen at 60 mm and 80 mm of distance between the yokes. At these two points, both of the yokes for structure 1 and 2 are located right in front of the vertical rebars.

Furthermore, dense meshing of the rebars can offer the feasibility of greater robot manoeuvrability on a vertical plane. To demonstrate that, the adhesion module arranged as structure 1 is rotated a full 360 degrees along its centre of gravity and the adhesion force is measured at 30° intervals. Figure 13b shows the results and it can be seen that the adhesion force is at its lowest value of 148 N when the yokes are

rotated 90° and 270° from their initial upright position. From this, it can be deduced that the two yokes adhesion module can offer a robot the freedom to turn 360° and still maintain a minimum adhesion force of 140 N.

6 Prototype Design and Experimental Setup

To validate the simulation results and test performance of the adhesion modules, a magnetic adhesion system consisting of three N42 grade rare earth neodymium magnets were arranged as layout 1 and attached to a prototype climbing robot. The robot's dimension was 360 × 210 × 25 mm and each magnet's size was 50 × 50 × 12 mm with a 350 mm long yoke. Wheeled locomotion was chosen for higher velocity and manoeuvrability compared to other locomotion techniques [30]. Each wheel was independently driven using servo motors capable of delivering 2.16 Nm of torque at 30 rpm. The wheel's outer diameter was 63 mm and sufficient enough to keep the air gap between the magnet face and the concrete surface at 2 mm as a small gap increases the adhesion force significantly. The robot's net weight was 2.23 kg and 3.68 kg for a 5 mm and 15 mm thick yoked robot respectively. The robots required 46 N and 76 N of force for sliding avoidance (obtained by using Eqs. 1 and 2 when acceleration, $a = 0.5\,m/s^{-2}$ and wheel friction coefficient, $\mu = 0.5$). The robot was equipped with four strain gauge based load cells capable of measuring up to 1500 N each. Load cells were affixed underneath the robot's chassis and the adhesion module was suspended freely in the loading platform using extensions which were secured in place to avoid displacement using additional screws. As the adhesion module presses toward the buried rebar, it applies force in the loading area of each load cell. The load cells produce a low-voltage milli-volt (mV) relative to the force applied. An operational amplifier HX711 was used to amplify the voltage and a AVR microcontroller based 10-bit analogue to digital module was used to convert the signals to numerical values and displayed on a computer screen using a Bluetooth data transmission system. A block diagram of the robot assembly and the prototype robot is shown in Fig. 14.

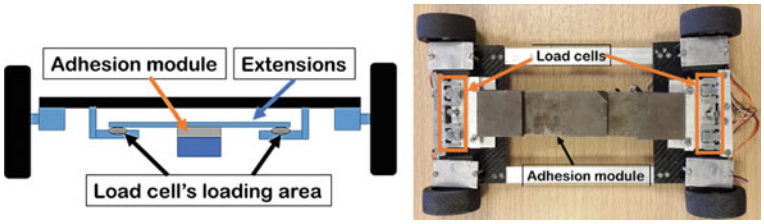

Fig. 14 Block diagram of the robot assembly and bottom view of the built prototype robot

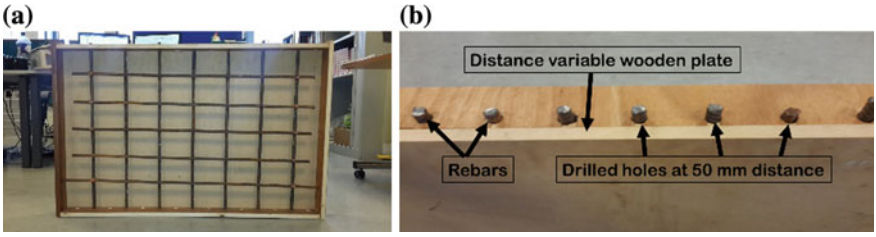

Fig. 15 Constructed experimental rig using wood frame and steel rebars: **a** Front view; **b** Top view

A test rig as in Fig. 15 was constructed to emulate a vertical reinforced concrete surface. 12 mm diameter holes were drilled along the length of a 1 m long and 70 cm tall wooden frame as the rebar holder. Distance between the rebars could be varied from 50 to 200 mm to investigate the effect of nearby rebars on adhesion force by slotting the rebars in through different holes. A 30 mm thick wooden plate simulating the concrete cover was also attached to the frame with screws which could be moved forward and backward using a slider to change the air gap.

7 Performance Validation of the Prototype Robot

To validate the performance of the prototype robot, experiments were carried out using the test rig at different rebar meshing and different air gaps. Measurements were taken at three different test points along the height of the test rig and the average value was considered. Force measurements were also recorded for rotational movements of the robot.

Firstly, the adhesion force was measured for 50 × 50 mm, 100 × 50 mm, 150 × 50 mm and 200 × 50 mm of rebar meshing with 30 mm air gap. The robot was positioned such that the adhesion module is aligned face-to-face with a vertical rebar. The robot's position was not changed while the rebar mesh settings were changed. Results shown in Fig. 16a suggest that when the rebars were densely meshed at 50 × 50 mm, highest adhesion force of 108.5 N could be achieved. In this case, the adhesion module could attract the front rebar as well as the adjacent vertical rebars located on its left and right side. As the distance increased to 100 mm, the module was only coupled with the front set of rebar and the next set of rebars were further apart to have any effect. At this stage, the adhesion force was 96.3 N. A further increase in the distance had no effect on the adhesion force which stayed at an average value of 95 N throughout.

For testing of rotational movements, the robot was rotated 360° along its centre of gravity and the resultant force was measured for different settings of rebar mesh. Figure 16b shows the respective results and according to that for 50 × 50 mm meshing, the adhesion force fell to a minimum value of 74 N at 60°, 120°, 240°, 330° of rotations. In these cases, the adhesion module was not aligned face-to-face with the

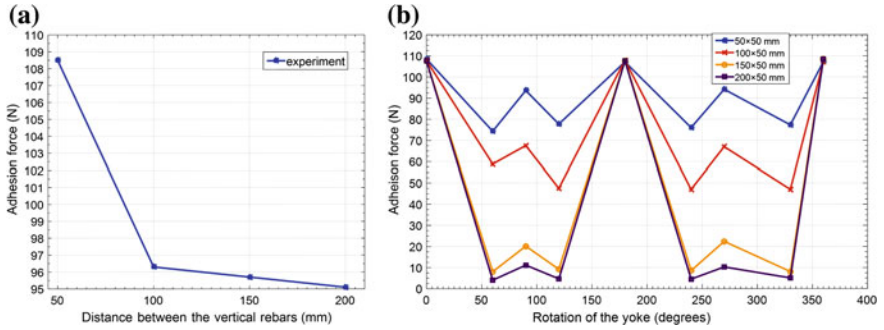

Fig. 16 Experimental results if the prototype: **a** Adhesion forces at different distances between the vertical rebars; **b** Adhesion forces at different rotations

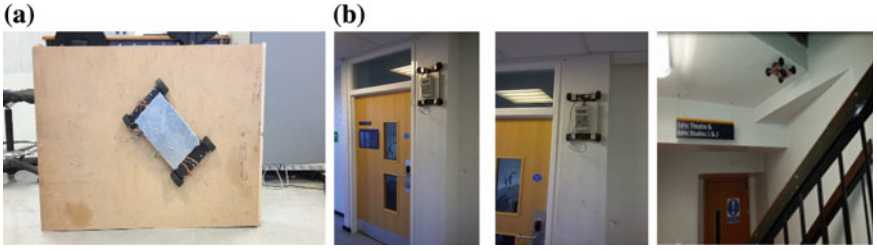

Fig. 17 **a** The prototype robot turning on the vertical test rig; **b** Climbing concrete column and ceiling with on board magnetic field sensor

rebar and as a result magnetic flux distribution was uneven. The same pattern was found for other setups. However, adhesion forces at 60°, 120°, 240°, 330° of rotation were decreasing with less dense meshing. The maximum adhesion force was at the same level of 108 N regardless of meshing settings while the module was aligned with a vertical rebar.

The robot was tested on the concrete column of a residential building. The rebars were reinforced in a 50 × 150 mm meshing at 30 mm depth. The concrete cover was measured using a concrete cover meter. The robot was carrying a Hall-Effect sensor as a payload that could identify the rebar location. The average adhesion force was measured to be 110.16 N with a maximum value of 127.53 N. The weight of the attached Hall-Effect sensor was 1.6 kg. Pictures of the robot climbing various surfaces are shown in Fig. 17. Adhesion force for different yoke thicknesses at a constant concrete cover of 30 mm also matched the same results achieved in simulations. Moreover, using thicker yokes resulted in higher adhesion forces as expected from simulations. However, increased weight of the yoke had a reverse relationship to the force-to-weight ratio. Figure 18 shows a gradual fall of η from 7.413 to 0.747 as the yoke thickness increased from 15 mm to 50 mm. Therefore, the yoke thickness of 15 mm should b an optimum design trade-off.

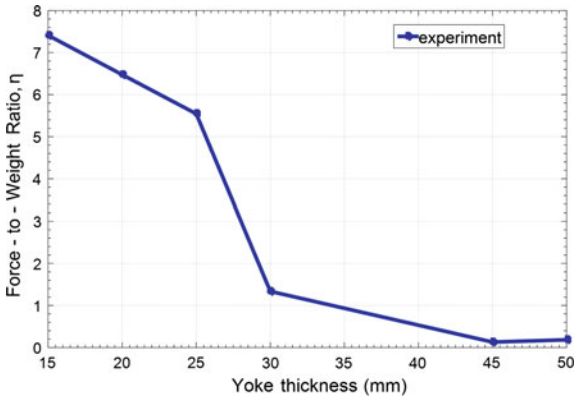

Fig. 18 Experimental values of force-to-weight ratios for different yokes used

8 Conclusion

Considering the workspace of the concrete wall climbing robot and safety requirements, a small size robot with high payload capacity has been presented in this chapter. Increased adhesion force has been achieved by arranging rare earth magnets on the back of a flux concentrator in a unique way and the robot's mechanical design ensures attachment of the magnet arrays at a constant distance from the surface while exhibiting small turning resistance. FEA based simulations have been carried out for parametric study of design variables. Distance between nearby magnets, yoke distance, number of yokes used were found to be the deciding factors of good performance. It was seen that by using two yokes, adhesion force could be maximized by 60 % compared to a single yoke system without compromising the force-to-weight ratio. To validate the simulation results, a prototype robot was built that was capable of displaying real time adhesion force values. Experiments on a test rig demonstrated the viability of 360° maneuverability of the robot on a reinforced rebar mesh surface. The minimum adhesion force was found to be 74.7 N on a 50 × 50 mm meshed surface when the robot is rotated around the vertical axis. This dense meshing was the only scenario where the robot was capable of completing a full 360° rotation. For other mesh settings, adhesion forces were critically low for full maneuvering. Though 12 mm diameter rebar was used for experiments, rebars used in the planned target application such as nuclear power plants have thicker rebars (up to 55 mm) and much denser meshing of the rebars making this method very feasible. Finally, 127.53 N of maximum adhesion force was measured with the robot climbing a real concrete column with 30 mm concrete cover while carrying 1.6 kg of additional payload. Higher grade (N52) of neodymium magnets could be used that will increase adhesion, while keeping the net system weight the same as N42 grade magnets. Considering the size, weight and high payload capacity of the robot, this is a practical solution for achieving zero-power permanent magnet based adhesion mechanisms for reinforced concrete environments.

References

1. Sattar, T., Hernando, E., Jianzhong, S.: Amphibious NDT robots. Int. J. Adv. Robot. Syst. **6**, 24 (2007)
2. Marceau, M., Michael, A., Vangeem, G.: Life Cycle Inventory of Portland Cement Concrete. Portland Cement Association, Skokie (2007)
3. Kosmatka, S., Kerkhoff, B., Panarese, W.: Design and Control of Concrete Mixtures. Portland Cement Association, Skokie (2008)
4. Sattar, T.P., Leon Rodriguez, H.E., Hussain, S.: Keynote paper: robotic non destructive testing. In: Proceedings of 26th International Conference on CAD/CAM, Robotics and Factories of the Future, Kuala Lampur (2011)
5. Garcia Ruiz, A., Sattar, T.P., Correa Sanz, M., Rodriguez-Filloy, B.S.: Inspection of floating platform mooring chains with a climbing robot. In: 17th International Conference on Climbing and Walking Robots and the Support Technologies for Mobile Machines, Poznan (2014)
6. Case Study on Oil and Gas: Comparison Between Rope Access and Scaffolding on 70 m Radio Tower Refurbishment. Megarme, Zirku Island (2011)
7. GSSI Case Study: A Tall Order: Scanning a 300-feet Chimney. Geophysical Survey Systems Inc, Salem (2009)
8. Zhiqiang, B., Yisheng, G., Shizhong, C., Haifei, Z., Hong, Z.: A miniature biped wall-climbing robot for inspection of magnetic metal surfaces. In: IEEE International Conference on Robotics and Biomimetics, Guangzhou (2012)
9. Bogue, R.: Robots in the nuclear industry: a review of technologies and applications. Ind. Robot: An Int. J. **38**(2), 113–118 (2011)
10. David, R., Elisabeth, C., Robert, D., Michael, G., Jacqueline, O.: Risk of cancer from occupational exposure to ionising radiation: retrospective cohort study of workers in France, The United Kingdom, and The United States (INWORKS). Br. Med. J. **351**, 5359 (2015)
11. Bayten, G.: Computerized Ultrasonic Inspection of LPD Vessel Construction Welds. Integrity NDT, Ankara (2012)
12. Zelihang, X., Peisun, M.: A wall climbing robot for labeling scale of oil tank's volume. Robot. Camb. J. **2**(2), 209–212 (2002)
13. Shang, J., Bridge, B., Sattar, T., Mondal, S., Brenner, A.: Development of a climbing robot for inspection of long weld lines. Ind. Robots Int. J. **35**(3), 217–223 (2008)
14. Kalra, P., Jason, G., Max, M.: A wall climbing robot for oil tank inspection. In: IEEE International Conference on Robotics and Biomimetics, Kunming (2006)
15. Zhang, Y., Dodd, T.: Design and optimization of magnetic wheel for wall and ceiling climbing robot. In: International Conference on Mechatronics and Automation, Xi'an (2010)
16. Luk, B., Collie, A., Cooke, D., Chen, S.: Walking and climbing service robots for safety inspection of nuclear reactor pressure vessels. In: Asia Pacific Conference on Risk Management and Safety, Hong Kong (2005)
17. Kim, H., Kim, D., Yang, H., Lee, K., Seo, K., Chang, D., Kim, J.: Development of a wall-climbing robot using a tracked wheel mechanism. J. Mech. Sci. Technol. **22**(8), 1940–1948 (2008)
18. Albagul, A., Asseni1, A., Khalifa, O.: Wall climbing robot: mechanical design and implementation. In: WSEAS International Conference on Circuits, Systems, Signal and Telecommunications, Mexico City (2011)
19. Manuel, F., Tenreiro, J.: A survey of technologies and applications for climbing robots locomotion and adhesion, ISBN: 978-953-307-030-8: InTech (2010)
20. Elliot, M., Morris, W., Xiao, J.: City-climber: a new generation of wall-climbing robots. In: IEEE International Conference on Robotics and Automation, Florida (2006)
21. Bretl, T., Rock, S., Latombe, J., Kennedy, B., Aghazarian, H.: Free-climbing with a multi-use robot. In: International Symposium on Experimental Robotics, Singapore City (2004)
22. Spenko, M., Haynes, G., Saunders, J., Cutkosky, M., Rizzi, A.: Biologically inspired climbing with hexapedal Robot. J. Field Robot. **25**, 4 (2008)

23. Avishi, S., Tomer, A., Amir, S.: Design and motion planning of an autonomous climbing robot with claws. J. Robot. Auton. Syst. **59**, 1008–1019 (2011)
24. Jensen-Segal, S., Virost, W., Provancher, R.: ROCR: energy efficient vertical wall climbing with a pendular two-link mass-shifting robot. In: International Conference on Robotics and Automation, California (2008)
25. Tso, S., Feng, T.: Robot assisted wall inspection for improved maintenance of high-rise buildings. In: International Symposium on Automation and Robotics in Construction, Eindhoven (2003)
26. Fanella, D.: Design of low-rise reinforced concrete buildings based on 2009 IBC. In: ASCE/SEI 7–05, ACI 318–08. International Code Council, Washington DC (2009)
27. Charles, R., James, C., Anthony, T.: Reinforced Concrete Designer's Handbook, 11th edn. Taylor and Francis Group ISBN: 9780419258308 (2007)
28. Design of Concrete Structures, General Rules. Eurocode 2, European Standard (2004)
29. Howlader, M., Sattar, T.: Novel adhesion mechanism and design parameters for concrete wall-climbing robot. In: SAI Intelligent Systems Conference, London (2015)
30. Schmidt, D., Berns, K.: Climbing robots for maintenance and inspections of vertical structures–a survey of design aspects and technologies. Robot. Auton. Syst. **61**(12), 1288–1305 (2013)